Chapter Number

Application of Microsystems Technology in the Fabrication of Thermoelectric Micro-Converters

L.M. Goncalves and J.G. Rocha
University of Minho, Guimarães, Portugal

1. Introduction

The use of thin-film deposition techniques with microsystems technologies renewed the interest in the thermoelectricity in the last years. Integration of efficient solid-state thermoelectric (TE) microdevices with microelectronics is desirable for local cooling and, since they can be used to stabilise the temperature of devices, decrease noise levels and increase operation speed. Their use in thermoelectric microgeneration (energy harvesting) can also supply energy to low power consumption electronic devices. In this chapter, the fabrication of thermoelectric microconverters is compared, both on materials from thin-film composites to supperlattice structures, and on its fabrication techniques.

Various materials can be used for this type of converters. However, for room temperature application, Bi/Sb/Te compounds are still the most efficient thermoelectric materials. Recently, efforts were made to apply quantum confinement to thermoelectric materials, and the results are thin-film superlattice structures and nanowires and even more recently, bulk nanocomposites. Some of these materials proved the ability to double efficiency of current thermoelectric devices. Several deposition techniques can be used for the fabrication of Bi/Sb/Te thin-films: co-sputtering, electrochemical deposition, metal-organic chemical vapor deposition or flash evaporation are some examples compared here.

The patterning process must use photolithography techniques to create the small dimensions of these devices. Despite these techniques are commonly used in microelectronic devices, mainly with silicon based substrates, its application in other thermoelectric alloys is still under development.

The patterning of thermoelectric structures for the fabrication of thermoelectric microconverters can be done using common microsystems technologies. Techniques used in MEMS fabrication, namely wet-etching, lift-off (with SU-8 photoresist), Reactive Ion Etching (RIE) and Lithography-Electroplating-Molding (LIGA) are here compared for the fabrication of thermoelectric microsystems.

2. Theory behind thermoelectric devices

There are two groups of applications for thermoelectric materials based on Seebeck and Peltier effects respectively. In the Seebeck effect, a temperature difference between the junctions of two different materials produces an electric voltage (figure 1), and an electric

current flows when the electric circuit is closed (Seebeck, 1882). This effect is quantified by the Seebeck coefficient, α, as represented in eq. 1:

$$\alpha = \frac{\Delta V}{\Delta T} \ (VK^{-1}) \tag{1}$$

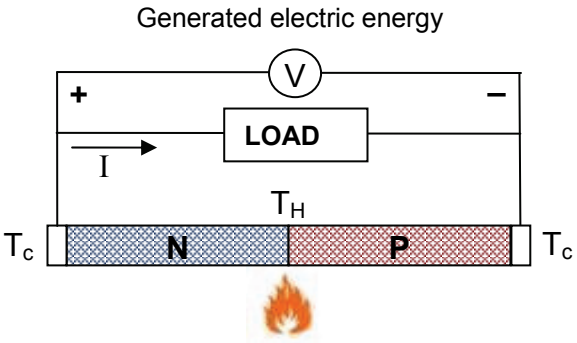

Fig. 1. In the Seebeck effect, a temperature difference between the junctions of two different materials makes an electric voltage to arise.

The Seebeck effect is used for two types of applications: temperature sensors and thermoelectric generators.

In the Peltier effect, when a current flow through the junction of two different materials, heat is absorbed or released in the junction, depending on the current direction (Peltier, 1834). This effect is quantified by the Peltier coefficient, π, related with the Seebeck coefficient (eq. 2):

$$\pi = \alpha T \tag{2}$$

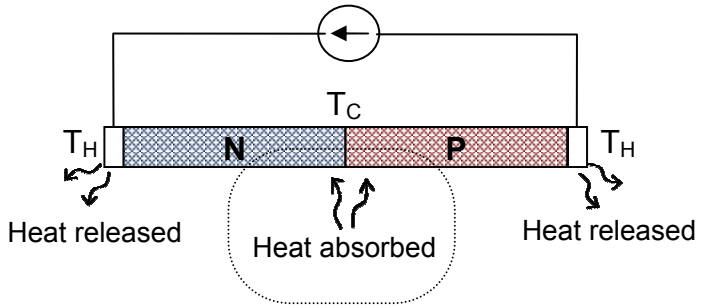

Fig. 2. In the Peltier effect, when a current flows through the junction of two different materials, heat is absorbed or released in the junctions.

The heat absorbed (Q_C) in the centre junction of figure 2, by Peltier effect can be calculated with eq 3.

$$Q_c = \left(\alpha_p - \alpha_n\right) T_c I \tag{3}$$

Due to the current flowing in N and P materials and the interfaces between materials (contacts), heat is generated by joule effect (Q_J). Eq. 4 calculates the total heat generated, since R represents the total resistance of the Peltier device.

$$Q_J = RI^2 \tag{4}$$

The complete model of a Peltier device (Wijngaards, 2000) can be considered as in figure 3. The electrical model (on the left of figure 3), includes the electrical equivalent resistance of the device (R), a voltage source that provides power to the device and a voltage source modelling the Seebeck effect of junctions, $(\alpha_p - \alpha_n)(T_h - T_c)$. The resultant current is I_e. On the right side of figure 3, the, thermal model is presented. The two current sources, $(\alpha_p - \alpha_n)I_eT_c$ and $(\alpha_p - \alpha_n)I_eT_h$, represent the cooling and heating by Peltier effect, respectively. The capacitors $C_{t,c}$ and $C_{t,h}$ are the heat capacity of on cold side and hot side and resistances $R_{t,c}$ and $R_{t,h}$ are the losses by convection and radiation to ambient temperature, T_a. $R_{t,h}$ is usually very small, and $T_h \approx T_a$. $R_{t,d}$ represents half of the thermal resistance between hot side and cold side. Q_j and Q_{jc} represent the heating by Joule, respectively on the thermoelectric materials and contacts. The load applied on the cold side of the device is represented by Q_L.

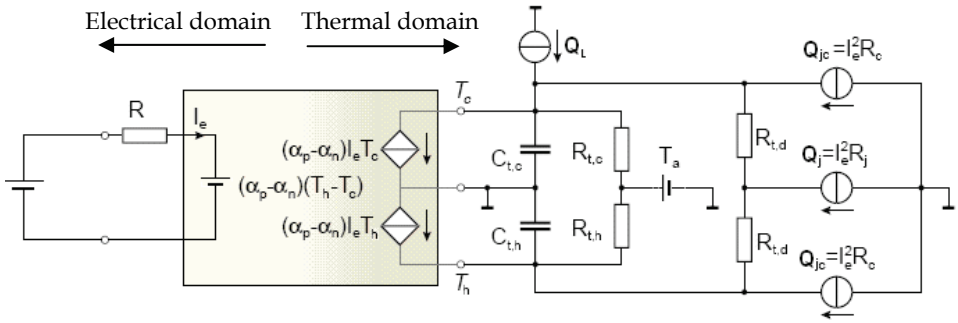

Fig. 3. Complete model of a Peltier microcooler, including electrical and thermal domains.

The same model can be used in an electrical power generator application, based on Seebeck effect, as figure 1. Instead of a voltage source (on the left side of the model in figure 3), a load is connected and the heat to convert to electrical energy (Q_L) is applied to the hot side of the device (T_h). The voltage generated is proportional to the temperature difference: $V=(\alpha_p - \alpha_n)(T_h - T_c)$.

Once each thermoelectric pair can produce a voltage near 400 μVK^{-1}, many pairs, connected in series, are necessary to generate a usable voltage. The maximum power in a thermoelectric generator, calculated with eq 5, is obtained when the load resistance equals the internal resistance (R).

$$P_{MAX} = \frac{V_{OUT}^2}{4R} = \frac{\left(n\left(\alpha_p - \alpha_n\right)\Delta T\right)^2}{4n\left(R_n + R_p + R_j + 4R_c\right)} \tag{5}$$

where n is the number of elements (pairs of thermoelectric p-n junctions), α is the Seebeck coefficient, ΔT is the temperature difference between the hot side and cold side of

thermoelectric elements (T_h- T_c) and R is the electric resistance. The indexes p and n refer to p-type and n-type materials respectively and the indexes j and c refer to materials of contacts and the contact itself. In order to obtain the maximum power, it is also important do match the thermal resistance of the generator with the heat sink (on the cold side) and hot object (in the hot side), not represented in the previous equation. In several applications, it is also important to analyze the impact of the generator in the temperature of the hot object. If a human-body generator is designed, it will not suit comfortable if much thermal power is absorbed from the skin (the sensation of cold will be noticed). By the other hand, when designing a thermoelectric generator for waste heat recovering (ex. recovering heat from a laptop CPU), an increase of temperature could occur where the heat is generated.
The coefficient of performance (COP) of the Peltier coolers is four to five times below to those found in conventional coolers (based on the Carnot cycle). Additionally, the unitary limit of the figure-of-merit (ZT - a performance measure of TE materials) it was seemed as an impossible barrier to pass, but also unexplainable. Bismuth telluride (Bi_2Te_3) and antimony telluride (Sb_2Te_3) compounds, were known for decades as the best thermoelectric materials at room temperature. Figure-of-merit is calculated by eq. 6.

$$Z = \frac{\alpha^2}{\rho k} \tag{6}$$

where α [μVK^{-1}] is the Seebeck coeficient, ρ [Ωm] is the electric resistivity and κ [Wm^{-1}K^{-1}] is the thermal conductivity. Figure-of-merit can also be calculated for a specific temperature, including T (absolute temperature) in the previous equation, resulting ZT:

$$ZT = \frac{\alpha^2}{\rho k} T \tag{7}$$

In thermoelectric generation applications, the power factor is sometimes used instead of figure-of-merit:

$$PF = \frac{\alpha^2}{\rho} \tag{8}$$

3. Materials for thermoelectric applications

Despite the continuous efforts in the search of an adequate material for fabrication of Peltier effect devices, more than 50 years ago that the value close to one of the figure-of-merit (ZT) seems to appear as a goal that can not be overtaken at room temperature. A good thermoelectric material must have high Seebeck coefficient, low electric resistivity and low thermal conductivity. But these three parameters are correlated. A material with low electric resistivity (a metal for example) frequently has a high thermal conductivity. The thermal conductivity based in the electronic transport (κ_e), which it is the dominant mechanism of thermal conduction in metals, is related with the electric conductivity (σ) by the Wiedemann-Franzem law, where L is the Lorenz number and T the temperature:

$$\frac{\kappa_e}{\sigma} = LT\,. \tag{9}$$

Theoretically, the Lorenz number is equal to:

$$L = \frac{\pi^2}{3}\left(\frac{k_B}{e}\right)^2 \approx 2.44 \times 10^{-8}\ \mathrm{W\Omega K^{-2}} \tag{10}$$

where k_B is the Boltzmann constant and e is the electron charge.
Figure 4 shows the figure-of-merit (Z) calculated for different materials at different temperatures.

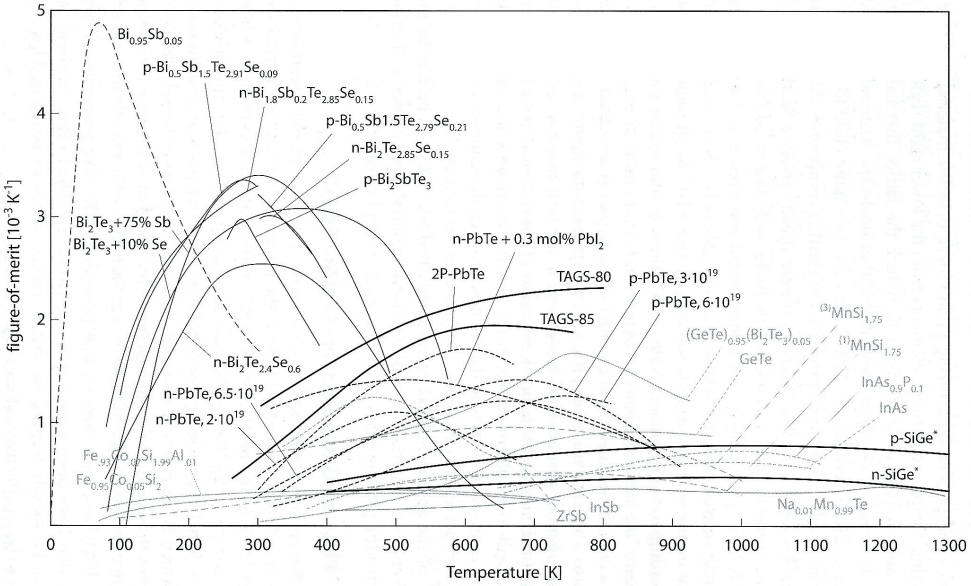

Fig. 4. Figure-of-merit (Z) calculated for different materials at different temperatures (Wijngaards, 2003).

Of the great number of materials investigated, those based on bismuth telluride, lead telluride and silicon-germanium alloys emerged as the best for operating at temperatures near 300 K, 900 K and 1400 K respectively.
Near the room temperature (250-350 K), tellurium (Te), bismuth (Bi), antimony (Sb) and selenium (Se) composites show the highest figure-of-merit values. For this reason, they are used in many of the commercial Peltier devices. The thermoelectric properties at room temperature of some of these materials are displayed in table 1.
For operation at temperatures around 800 K, lead antimony telluride shows the highest figure-of-merit. A ZT value around 1 was reported at 800 K (Fano, 1997). However, there are environmental restrictions to the use of lead. Silicon-Germanium is a candidate material for operation at temperatures above 1000 K. A figure-of-merit around unity was achieved at 1200 K (Vining, 1997). These materials also have the advantage of easy integration with microelectronics.

Material	*Symbol*	*Seebeck coefficient a (μVK⁻¹)*	*Resistivity ρ (μΩm)*	*Thermal conductivity κ (Wm⁻¹K⁻¹)*	*Figure of merit ZT*	*Temperature K*
Nickel	Ni	-18	0.070	91	0.015	300
Chromium	Cr	18	0.13	94	0.008	300
Bismuth	Bi	-60	1.15	8.4	0.110	300
Antimony	Sb	40	0.42	18.5	0.062	300
Silicon-Germanium (n)	SiGe	-242	17.8	4.2	0.94	1200
Silicon-Germanium (p)	SiGe	240	31.9	4.38	0.50	1200
Bismuth telluride (n)	Bi_2Te_3	-240	10	2.02	0.86	300
Antimony telluride (p)	Sb_2Te_3	92	3.23	1.63	0.48	300

Table 1. Thermoelectric properties of some materials.

4. Quantum confinement in thermoelectricity

There are a lot of attempts to produce thermoelectric materials with ZT greater than one. Nevertheless, the best commercial thermoelectric modules, fabricated from bismuth, antimony and tellurium compounds, have ZT close to one. This is mainly due to the fact that in conventional 3D crystalline systems the Seebeck coefficient (α), the electrical conductivity (σ) and the thermal conductivity (κ) are interrelated, being difficult if not impossible to control each factor independently in order to improve ZT (Bottner, 2006; Bell, 2008). An increase of α, usually results in a decrease of σ. By the other hand, a decrease of σ leads to a decrease of the electronic contribution to κ. However, if the dimensions of the material decrease, a scale factor becomes available for the control of material properties (Hicks, 2003). This phenomenon is due to the reduction of the 3D solid crystalline structures to 2D superlattices (figure 5), 1D nanowires, or quantum dots, introducing new forms to control α, σ or κ more independently. The introduction of many interfaces in the structure can scatter phonons more effectively than electrons and allows enhanced ZT in such nanostructured materials. Recent work with PbTe (Harman, 2002), SiGe (Caylor, 2007) and BiSbTe (Bottner, 2006; Venkatasubramanian, 1992) superlattices demonstrated an enhancement of ZT. ZT=2.4 and ZT=1.4 were measured in p-type and n-type Bi/Sb/Te superlattices (Venkatasubramanian , 2001), respectively.

The use of thin-film processes in thermoelectric structures limits the thickness of deposited films to few micrometers. Using this thickness, the achieved heat-flow density has higher value, compared with traditional large scale devices. If 10 Wcm^{-2} can be found in typical large-scale devices, 500 Wcm^{-2} could be supported in a thin-film device. However, this density could not be attended with conventional heatsinks. For lower density applications, efforts are also being done to achieve bulk materials (rather than films) with increased figure-of-merit. A periodic structure is the major mechanism to reduce thermal conductivity and support the enhanced figure-of-merit in superlattices. However, nanocomposites become a natural step for extending the success in superlattices to more scalable materials. Randomly distributed nanostructures in nanocomposite materials (figure 6) can lead to a reduction in the thermal conductivity below that of an alloy of the same overall chemical stoichiometry (Dresselhaus, 2007). These materials can be prepared by either wet-chemistry, ball-milling, or by inert-gas condensation methods. Nanometer or micrometer sized particles are then hotpressed to obtain dense and mechanically strong, bulk nanocomposites.

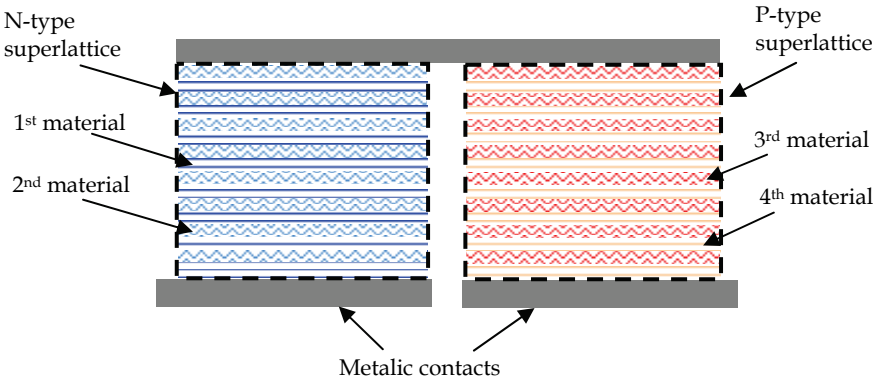

Fig. 5. Thermoelectric pair with superlattice materials. Each material is composed by alternating layers of two different materials, whose thickness is in the range of tens of nanometers.

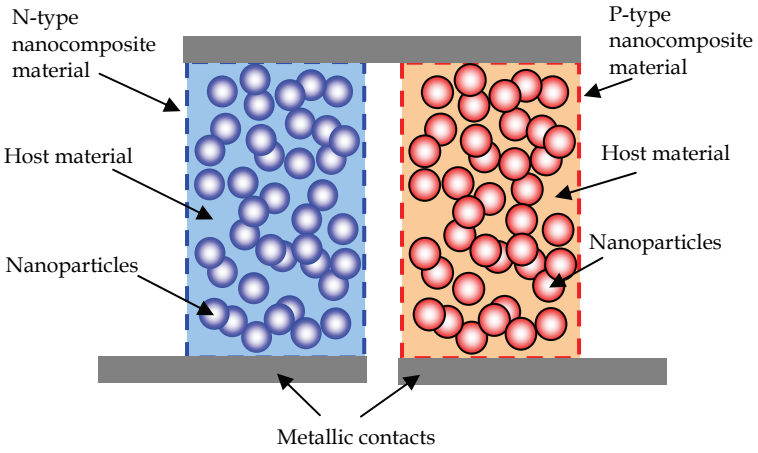

Fig. 6. Thermoelectric pair with nanocomposite materials.

There is also certain optimism concerning the materials of the group of clathrates, which create crystals with nanocages and whose thermal conductivity can be reduced if an atom of an heavy element is placed inside of cages.

The energy and environmental circumstances have relaunched the current research on these materials significantly. The results presented by a group of the University of Aarhus, the Copenhagen University and the Technical University of Denmark are part of this new wave and should help to accelerate research in the world. Their study describes why some materials may have very low thermal conductivity without degrading their electrical properties. Their research work has focused on the properties of one of the thermoelectric materials of the most promising family of clathrates, which the crystal is filled with nanocages. By placing a heavy atom in the heart of each nanocage, it is possible to reduce the ability of the crystal conduct heat. The research team thought that the random movements of atoms in the cage were

responsible for the phenomenon. They used the technique of neutron scattering which allows the observation of the movements of atoms within the material. They understood that the thermoelectric properties were determined by the global movement of nanocage structure, which is influenced by the heavy atom therein (Christensen, 2008).

5. Thin-film fabrication

A single junction of Bi_2Te_3-Sb_2Te_3 thermocouple has a Seebeck voltage of only 400 μVK^{-1}. To achieve a usable voltage in generator devices, more than 4000 thermocouples must be connected in series. If these 4000 thermocouples are to be fitted in a 1 cm^2 device, each thermocouple is about 100 μm × 200 μm. The fabrication methods used in macro-sized TE devices cannot be used in the fabrication of these micro-devices. In these devices, microsystems technology should be used instead. Materials can be deposited by thin-film deposition processes (physical and chemical vapour deposition or electrochemical deposition). Some techniques were tried before for the deposition of Bi/Sb/Te thin-films. Electrochemical deposition (ECD), metal-organic chemical vapour deposition (MOCVD), pulsed laser deposition (PLD), sputtering and thermal evaporation are some examples. Independently of the technique used, a good control of film composition and crystalline structure is very important to fabricate films with high figure-of-merit. Previous research (Goncalves, 2009), demonstrated the optimum composition to maximize figure-of-merit. A tellurium content in the range 60%-65% can maximize figure-of-merit. When evaporating directly the compounds (either Bi_2Te_3 or $Bi_xSb_{2-x}Te_3$), these elements decompose and the final composition of the deposited film does not match the composition of the initial target, due to different vapour pressure of each element (Bi, Sb or Te). Moreover, when thicker films are deposited, the composition differs from surface to deep film layers (Silva, 2005). This effect is more evident in thermal evaporation, since the increase in temperature promotes de decomposition of source materials. To overcome this problem, co-deposition systems (either thermal co-evaporation (Goncalves, 2007) or co-sputtering (Kim, 2006; Bottner, 2004)) are usually used, and the deposition rate of each element (Bi, Sb or Te) is controlled independently, in order to obtain the final optimal composition. The power factor of films deposited by co-evaporation, as function of composition (measured by EDX) and substrate temperature is presented in figure 7.

The importance of crystalline structure in figure-of-merit was also demonstrated before. The structure of these films changes from amorphous to polycrystalline. Films with a more crystalline structure have usually low electrical resistivity. The polycrystalline structure of these films also decreases the thermal conductivity (compared with a single crystal) (Scherrer, 1997) thus increasing the figure-of-merit. The crystalline structure can be controlled by the substrate temperature during deposition or with annealing cycles after deposition. However, due to different vapour pressure of tellurium, bismuth or antimony, the composition of the films can change with heating, resulting in films poor in tellurium. The influence of substrate temperature in films deposited by co-evaporation is presented in Fig 7. A low deposition rate (bellow 2 μm/h) also allows an appropriate crystallization, resulting in higher figure-of-merit. This low deposition rate limits the thickness of film that can be deposited. Using co-sputtering or ECD, higher deposition rate can be obtained. IPM (Bottner, 2004) reported a deposition rate of 5 μm/h using co-sputtering and JPL (Fleurial, 2003) fabricated a device with thermoelectric columns 20 μm high by ECD. Table 2 compares the thermoelectric properties of Bi_2Te_3 and $Bi_xSb_{2-x}Te_3$ films fabricated by different techniques.

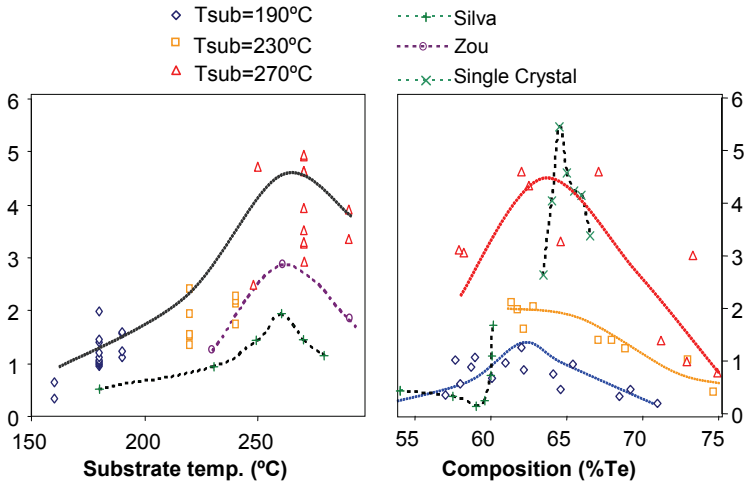

Fig. 7. The power factor of films deposited by co-evaporation, as functions of substrate temperature and composition (measured by EDX). Results from other authors and from single crystal are also presented.

Material		*Deposition technique*	*Seebeck a (μVK⁻¹)*	*Resistivity ρ (μΩm)*	*Power factor 10⁻³WK⁻²m⁻¹*	*Fig. of merit Z ×10⁻³K⁻¹*	*Reference*	*Obs*
Bi_2Te_3	n	Co-evaporation	-220	10.6	4.57	3.03	Goncalves, 2009	
Sb_2Te_3	p	Co-evaporation	188	12.6	2.81	1.87	Goncalves, 2007	
Bi_2Te_3	n	Electrochemical	-60	10	0.36	-	Lim, 2002	
Bi_2Te_3	n	MOCVD	-210	12	3.7	2.48	Giani, 1999	(1)
Sb_2Te_3	p	MOCVD	-110	3.5	3.46	-	Giani, 1999	
Bi_2Te_3	p	MOCVD	190	78	0.46	2.5	Giani, 1997	(1)
Bi_2Te_3	n	MOCVD	-218	6.9	6.9	-	Boulouz, 1998	
$Bi_{0.5}Sb_{1.5}Te_3$	p	Flash	230	17	3.1	2.9	Volklein, 1990	
$Bi_2Te_{2.72}Se_{0.3}$	n	Flash	-200	15	2.7	-	Foucaran, 1998	
$Bi_{0.5}Sb_{1.5}Te_3$	p	Flash	240	12	4.8	-	Foucaran, 1998	
$Bi_{1.8}Sb_{0.2}Te_{2.7}Se_{0.3}$	n	Sputtering	-235	47	1.2	-	Kessler, 2003	(2)
Bi_2Te_3	n	Co-Sputtering	-160	16.3	1.6	-	Bootner, 2004	(3)
$(BiSb)_2Te_3$	p	Co-Sputtering	175	12.1	2.5	-	Bootner, 2004	(3)
$Bi_2Se_{0.3}Te_{2.7}$	n	Sputtering	-160	20	1.3	-	Stordeur, 1997	
$Bi_{0.5}Sb_{1.5}Te_3$	p	Sputtering	210	25	1.8	-	Stordeur, 1997	
Bi_2Te_3	n	Co-Sputtering	-55	10	0.3	-	Kim, 2006	
Bi_2Te_3	n	Co-evaporation	-228	13.0	4.0	2.7	Zou, 2001	(1)
Sb_2Te_3	p	Co-evaporation	171	10.4	2.8	1.76	Zou, 2001	(1)
Bi_2Te_3	n	Co-evaporation	-228	28.3	1.8	-	Silva, 2005	
Sb_2Te_3	p	Co-evaporation	149	12.5	1.78	-	Silva, 2005	

Obs: (1) Z estimated by the author.
(2) Doped with CuBr.
(3) The power factor of de 3×10^{-3} $WK^{-2}m^{-1}$ and 4×10^{-3} $WK^{-2}m^{-1}$, respectively for type n and type p was reported latter by the same authors (Bottner, 2007) but no reference of other thermoelectric properties was found.

Table 2. Properties of selected Bi_2Te_3 and $Bi_xSb_{2-x}Te_3$ films

6. Patterning of devices

Common techniques used in MEMS fabrication, namely wet-etching, lift-off (with SU-8 photoresist), Reactive Ion Etching (RIE) and Lithography-Electroplating-Molding (LIGA) were tried before in the fabrication of thermoelectric microstructures.

IPM (Bottner, 2004) used RIE techniques to pattern thick films of Bi,Sb,Te materials, using photoresist as an etching mask. Two wafers with patterned thermoelectric materials were soldered to create the columnar thermoelectric device. Each wafer contains n-type or p-type materials, deposited on top of metal contacts and a soldering material deposited on top. The wafers are then aligned and soldered. This process allows the deposition of thermoelectric materials with crystalline structure by heating the substrate during the deposition of thermoelectric materials.

The JPL laboratory (Snyder, 2003) used a MEMS like process, LIGA, to fabricate micro-columns of TE materials. Gold-chromium contacts were deposited and patterned on the substrate. Thick photoresist was patterned to create holes were TE materials were deposited by ECD. A gold-nickel layer was then deposited and patterned over the structures to create top contacts. Photoresist, gold and chromium layer were etched, creating the complete device. By this process, height columns can be created, however the figure of merit of thermoelectric materials deposited by ECD is low.

Lift-off can also be used in thermoelectric materials. Photoresist is spun cast and patterned to define the lift-off pattern for thermoelectric materials that will be deposited on top. The photoresist is then removed, removing also the TE material on top of it and creating the structures. The process is repeated for each thermoelectric material. The technique was applied by Silva (Silva, 2005), using SU-8 photoresist and thermal co-evaporated Bi_2Te_3 and Sb_2Te_3 thin-films. Yield of this process was low, in particular with small TE elements (7 μm × 7 μm). Due to temperature limit of photoresist, substrate cannot be heated above 170 ^oC during the deposition of TE materials and the figure-of-merit is lower than these obtained at higher substrate temperatures.

Shafai (Shafai, 2001) reported the possibility of use nitric acid (HNO_3) and hydrochloric acid (HCl) diluted in water (H_2O) for etching Bi_2Te_3, but his work was not extended to full characterize this process, or apply it to other tellurium compounds. Recent work from Sedky (Sedky, 2009) also proposed suspended Bi_2Te_3 microstructures fabricated by wet-etching. Goncalves (Goncalves, 2007) deposited thin-films of Bi_2Te_3 and Sb_2Te_3 (1 μm thick) on polyimide substrates, by thermal co-evaporation. Transene's PKP negative photoresist was applied on the surface and test structures were patterned by photolithography. Different etching solutions were prepared (Goncalves, 2008) using water, pure HNO_3 and 37% HCl dil. in water and the effect of etchant composition in etch rate and final result was evaluated. Figure 8 plots the etch rate of Bi_2Te_3 and Sb_2Te_3 films in (1-x)HNO_3:(x)HCl solution (diluted 70% in water, in volume).

Higher percent of HCl (%HCl / %HNO_3 > 0.5) induces cracking of the film and peeling occurs. Using only HNO_3 (diluted at 70% in water) Bi_2Te_3 is etched at ≈300 nm/sec and the Sb_2Te_3 etch rate is below 6 nm/sec. This difference of 50× can be useful to pattern devices with both materials, etching Bi_2Te_3 with HNO_3 without etching Sb_2Te_3 films. However, this method cannot be used with $Bi_xSb_{2-x}Te_3$ instead of Sb_2Te_3. The behavior of $Bi_xSb_{2-x}Te_3$ is equivalent of Bi_2Te_3, even with small percentage of Bi in composition. Figure 9 plots the influence of etchant dilution (in water) in etch rate, respectively in Bi_2Te_3 and Sb_2Te_3 films.

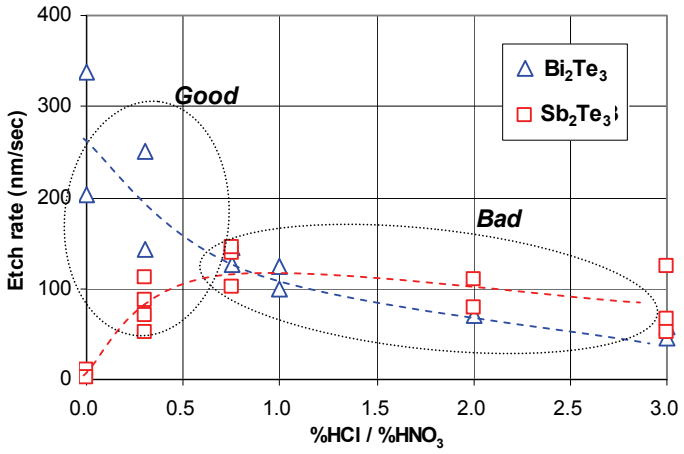

Fig. 8. Etch rate of Bi_2Te_3 and Sb_2Te_3 films in (1-x)HNO_3:(x)HCl solution (diluted 70% in water, in volume).

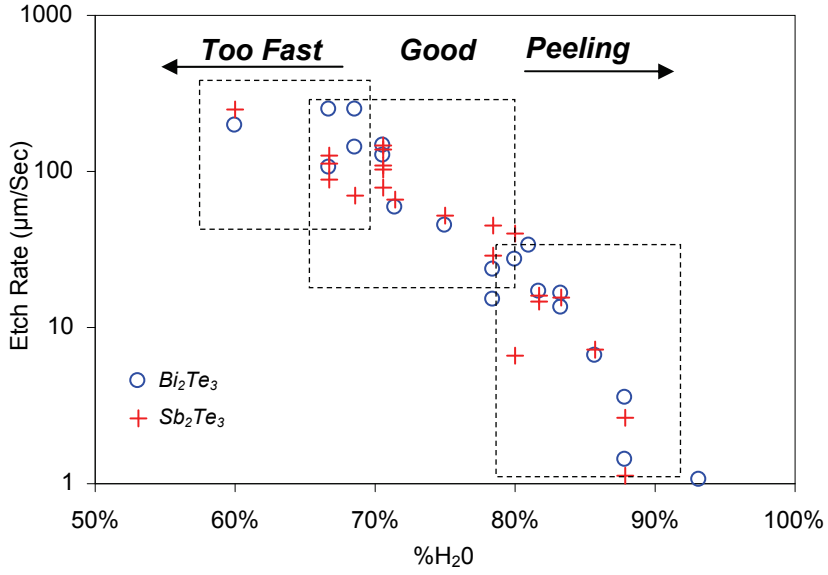

Fig. 9. Influence of dilution (in water) in Etch rate of Bi_2Te_3 and Sb_2Te_3 films in 10:3 HNO_3:HCl solution.

Etchant of composition with dilution of 70% produces the best results. With dilution above 80% in water, the etch rate is very low and peeling of the film occurs. With dilutions below 60%, the etch rate is very high and becomes difficult to control de etch time. Table 3 shows the etch rate of Bi_2Te_3, Sb_2Te_3, chromium and aluminum in HNO_3:HCl:H_2O, HNO_3, aluminum etchant (Transene type A) and chromium etchant (Transene 1020). The selectivity

between different etchants in different materials allows different possibilities to fabricate a complete device. Figure 10 shows the patterned structures used in etchant evaluation.

Etchant \ Material	Bi_2Te_3	Sb_2Te_3	Aluminum	Nickel
Al – Transene type A	8	5	10-80	< 0.1
Cr - Transene 1020	≈ 20	<1	-	10-40
$3HNO_3$:1HCl (dil 70% H_20)	2000	800	< 2	< 0.2
HNO_3 (dil 70% H20)	2500	50	< 0.1	< 0.1

Table 3. Summary of etch rates (Å /sec).

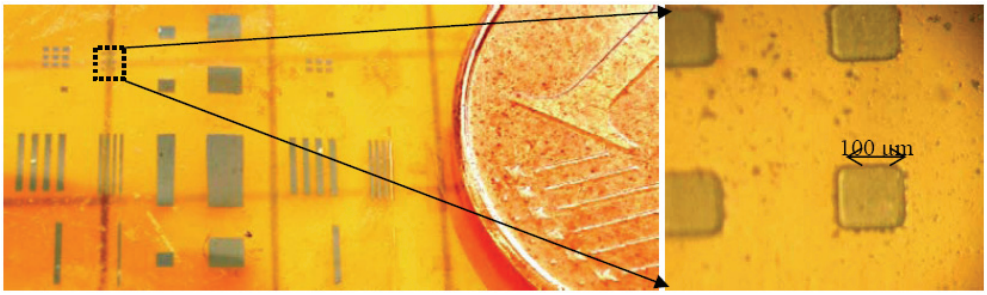

Fig. 10. Test structures of thermoelectric films patterned by chemical etching.

7. Applications

Thermoelectric materials have unique properties that make them useful to convert thermal energy into electric energy and vice-versa. For this propose, beyond a large Seebeck coefficient, they must have high electrical conductivity and low thermal conductivity. Despite this two properties being related, Bi/Sb/Te compounds are the best materials for thermoelectric applications at room temperature. This applications fall in two main categories: Cooling and electric energy generation.

In recent years, the available air conditioners and refrigerators have become a way of life for millions of people around the world. At the same time, energy costs and environmental regulations regarding the manufacture and release of CFCs are also increasing. These facts are encouraging manufacturers and their customers to seek alternatives to conventional refrigeration technology. Despite the performance of thermoelectric cooling being far from Carnot cycle compressors, some specific application requiring low maintenance, long life with no moving parts are using thermoelectric refrigeration.

Regarding generator applications, the use of thermoelectric devices in vehicles is currently being addressed. Thermoelectric converters can be used in cars, in order to make the engines most efficient. A conventional combustion engine wastes about 80% of the energy of the fuel under the form of heat. The thermoelectric devices can be directly used to generate electric energy from this wasted heat. A fuel consumption reduction of 10% is achievable, which represents a significant impact in the global energy spent in transport of people and goods all over the world. Using thermoelectric materials, this heat can be used to produce electrical energy, which in turn can be used to charge the car battery.

Small sized applications, from few cubic-centimetres to few cubic micrometers are not realizable with Carnot cycle compressors. In these low-power applications, thermoelectric devices are applied with advantages. The same thermoelectric principle can be used to build cooling systems inside microchips, optimizing the heat sink capability. These small devices can also be used to control temperature of sensible electronic circuits.
The micro thermoelectric generators have applications in energy harvesting microsystems. From low temperature gradients found in human-body or house environments, energy can be generated to power wireless devices. Self-powered wrist-rings for watch or sensor applications or thermoelectric bolts, that can generate energy wherever they attach, are being developed to power-up microwatt electronic circuits.

8. References

Bell, L. (2008). Cooling, heating, generating power, and recovering waste heat with thermoelectric systems. *Science*, 321, pp. 1457-1461.

Bottner, H. et al (2004). New thermoelectric components using microsystem technologies, *Journal of Microelectromechanical System* 13 Issue 3, pp. 414 – 420.

Bottner, H. et al (2007). New high density micro structured thermogenerators for stand alone sensor systems, *in Proc. International Conference on Thermoelectrics ICT'07*, Korea.

Boulouz, A. et al (1998). Preparation and characterization of MOCVD bismuth telluride thin films, *J. Crystal Growth* pp. 194 336.

Dresselhaus M. S. et al (2007). New Directions for Low-Dimensional Thermoelectric Materials, *Advanced Materials* 19, 2007

Fano, V. (1987). CRC handbook of thermoelectrics, edited by D.M. Rowe, 261.

Foucaran, A. et al (1998). Flash evaporated layers of (Bi2Te3–Bi2Se3)(N) and (Bi2Te3–Sb2Te3)(P), *Materials Science and Engineering B* 52, pp. 154–161.

Giani, A. et al (1997). Bi2Te3 films grown by MOCVD, *Thin Solid Films*, Vol 303 (1997) 1-3.

Giani, A. et al (1999). Growth of Bi2Te3 and Sb2Te3 thin films by MOCVD, *Materials Science and Engineering B* 64, pp. 19–24.

Goncalves L. M. et al, (2007). Fabrication of flexible thermoelectric microcoolers using planar thin-film technologies, *Journal of Microelectromechanical Systems* 17.

Goncalves, L. M. et al (2008). Thermoelectric Micro Converters for Cooling and Energy Scavenging Systems" *Journal of Microelectromechanical Systems* 18.

Goncalves L. M. et al (2009). *Thin Solid Films,* In press.

Harman TC, Taylor PJ, Walsh MP, LaForge BE, (2002). Quantum Dot Superlattice Thermoelectric Materials and Devices, *Science* Vol. 297. no. 5590, pp. 2229 - 2232

Hicks D. and Dresselhaus M. S. (1993). Effect of quantum-well structures on the thermoelectric figure of merit. *Physical Review B: Condensed Matter*, 47, 12727-12731

Kessler, E. et al (2003). Thin-film infrared thermopile sensors with thermoelectric high-effective materials combination. *Proceedings of Sensor 2003*, 11th International Conference, Vol. II, Nürnberg 249-254.

Kim, Ding-ho et al (2006). Effect of deposition temperature on the structural and thermoelectric properties of bismuth telluride thin films grown by co-sputtering. *Thin Solid Films*, 510 148-153.

Lim, J.R. et al (2002). Thermoelectric Microdevice Fabrication Process and Evaluation at the Jet Propulsion Laboratory (JPL), i*n Proc. International Conference on Thermoelectrics.*

Mogens Christensen et al (2008). Voided crossing of rattler modes in thermoelectric materials, *Nature Materials*, Vol. 7, (10) pp. 811 – 815.

Peltier, J. C. (1834). Nouvelles experiences sur la caloricité des courans électriques. *Annales de Chimie et the Physique*, LVI 56, pp. 371-386.

Scherrer, H. and Scherrer, S. (1987). CRC handbook of thermoelectrics, edited by D.M. Rowe, pp. 211-237.

Sedky, Sherif et al (2009). Bi2Te3 as an active material for mems based devices fabricated at room temperature, *in Proc. International Conference Transducers09*, Denver, Colorado USA

Seebeck, T. I. (1822). Magnetische polarisation der metalle und erze durch temperatur-differenz. *Abhandlungen der Deutschen Akademie der Wissenschaften zu Berlin*, pp. 265-373.

Shafai, C. and Brett, M.J. (2001). Optimization of Bi2Te3 thin films for microintegrated Peltier heat pumps, *Journal of Vaccum Sci Technol A*, Vol. 17- 1 pp. 305-309.

Silva, Luciana; Kaviany, Massoud and Uher, Citrad (2005), *Journal of Applied Physics* 97, pp. 114903.

Snyder, G. Jeffrey et al (2003). Thermoelectric microdevice fabricated by a MEMS-like electrochemical process, *Nature Materials* 2 pp. 528.

Stordeur, Matthias and Stark, Ingo (1997). Low Power Thermoelectric Generator - self-sufficient energy supply for micro systems. *16th International Conference on Thermoelectrics*.

Venkatasubramanian, R. et al. (1992). *in Proc. 1st Natl Thermogenic Cooler Workshop*. Center for Night Vision and Electro-Optics, Fort Belvoir, VA, pp. 196-231.

Venkatasubramanian, R. et al. (2001). Thin-film thermoelectric devices with high room-temperature figures of merit. *Nature*, pp. 413.

Vining, Cronin B. (1987). CRC handbook of thermoelectrics, edited by D.M. Rowe, 329.

Völklein, F. et al (1990). Transport properties of flash-evaporated (Bi1-xSbx)2Te3 films: Optimization of film properties, *Thin Solid Films* 187 pp. 253-262.

Wijngaards D.D.L.; Cretu E.; Kong S.H. and Wolffenbuttel R.F (2000). Modeling of integrated polySiGe Peltier elements, *Sixth THERMINIC Workshop*, Budapest, Hungary, 24–27 September (2000) 2 pp. 75a–275d.

Wijngaards, Davey (2003). Lateral on-chip integrated Peltier elements based on polycrystalline silicon germanium, *Phd Thesis*, Tu Delft.

Zou, Helin; Rowe, D.M. and Min, Gao (2001).Growth of p- and n-type bismuth telluride thin films by co-evaporation. *Journal of Crystal Growth*, Vol. 222 (2001) pp. 82-87.